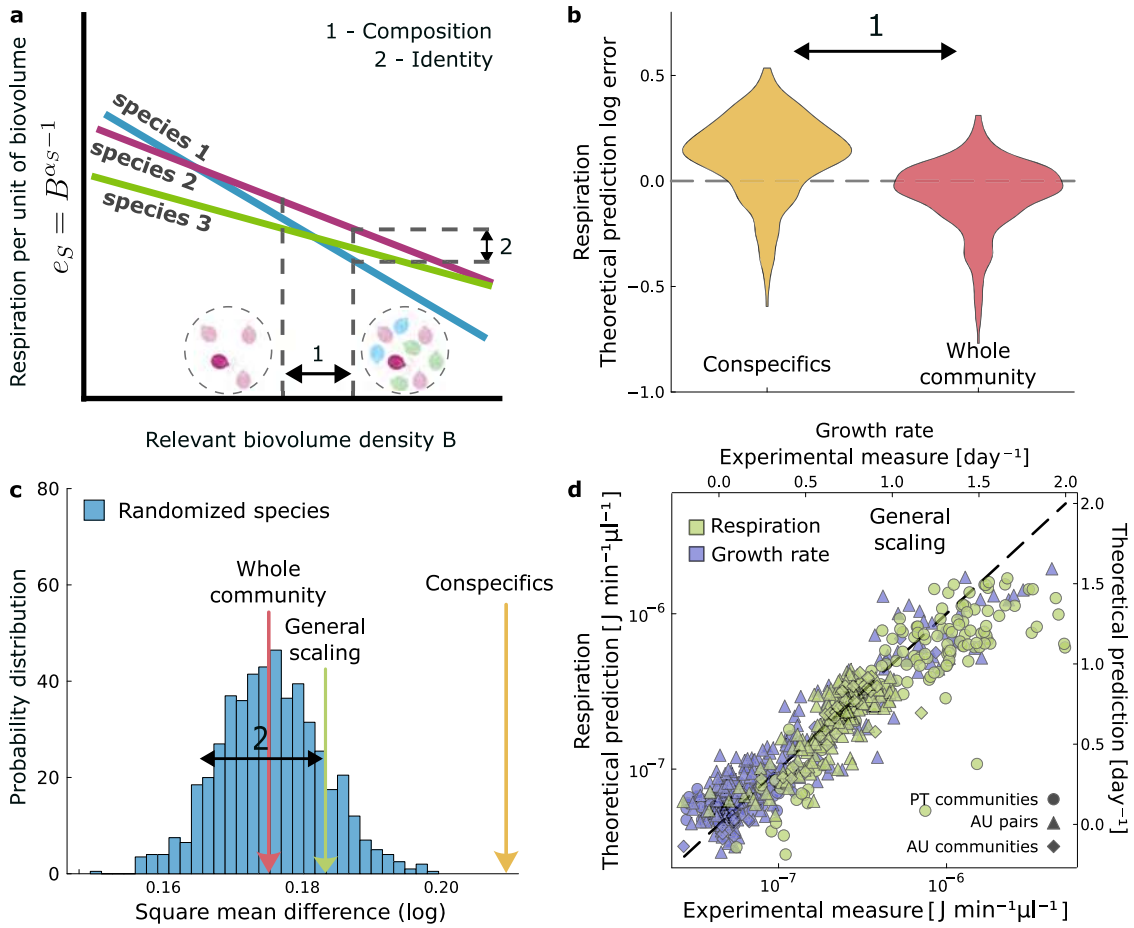

Fig. 3 | Predictions of community respiration based on different models of metabolic density-dependence. a Schematic showing species-specific declines in respiration rates per unit biovolume with increasing biovolume. We use these species-specific relationships, based on monoculture data in each environment, to test the importance of two factors on community metabolism: (1) biomass composition (are metabolic declines driven equally by intra- and inter-specific competitors?), (2) species identity (do species-specific differences considerably affect community rates?). **b** Error of the predictions testing factor 1. We can correctly estimate community respiration rates if we consider the total biovolume of the community. If we account only for conspecifics, we overestimate community rates. **c** Species identity (factor 2) does not significantly affect community respiration. If we randomise the association between species-specific declines in respiration and the biovolume of species in the community, we obtain a distribution of estimates (blue) that contains the prediction made using the correct association ("whole community", magenta). Predictions based on conspecifics are outside of this range. **d** Since species identity has minimal effects, we can estimate total community respiration (green) or growth (purple) using a general scaling between respiration (growth) per unit mass and total biomass across all species (green arrow in panel **c**, refers to respiration). Abbreviations: AU = Australia, PT = Portugal. See Supplementary Figs. 15 and 16 for growth and photosynthesis. Source data are provided as a Source Data file.

respiration and growth) and the fact that species-specific responses to light availability are more pronounced for photosynthesis than respiration (Supplementary Figs. 1, 2).

Environmental conditions highlight the link between community growth and metabolism

Community metabolism and growth slow as biomass increases independently of size composition across all the environments we considered. In this last section, we leverage differences in environmental conditions to explore the connection between these density-dependent rates. We focus on photosynthesis and growth because they both respond strongly to light availability, while this is less obvious for respiration (Supplementary Figs. 1, 2).

Light availability modifies the density-dependence of community growth and photosynthesis rates per unit biovolume, but these rates remain highly correlated within each environment (Fig. 4a, b). Furthermore, once we account for differences in light intensity (AU = 115 µmol photons m^{-2} s^{-1} > PT High = 60 > PT Low = 30), photosynthesis and growth rates converge across all environments (Fig. 4c). Both growth and photosynthesis thus respond to increases in biovolume in a very similar way, indicating a strong level of community regulation that holds across environments.

We cannot establish if photosynthesis metabolism governs growth or the other way around[24]. But our data show that biomass competition slows metabolism in a very similar and predictable fashion across species (Fig. 2) so that the density-dependent patterns observed in individual populations (Fig. 1)[18] extend to entire communities throughout their whole growth process (i.e., both when far and close to equilibrium; Fig. 4).

Discussion

Ecosystem productivity scales predictably with total biomass, independently of species size and composition[3]. These size-independent patterns seem incompatible with the sublinear scaling of growth and metabolism observed at the individual level within most taxa[5,10,26]. We demonstrate the connection between these scalings by showing that biomass competition influences organismal metabolism identically across species of different sizes that compete for similar resources. These species grow, photosynthesise and respire at different rates per unit mass when compared at equal population densities, thus focusing

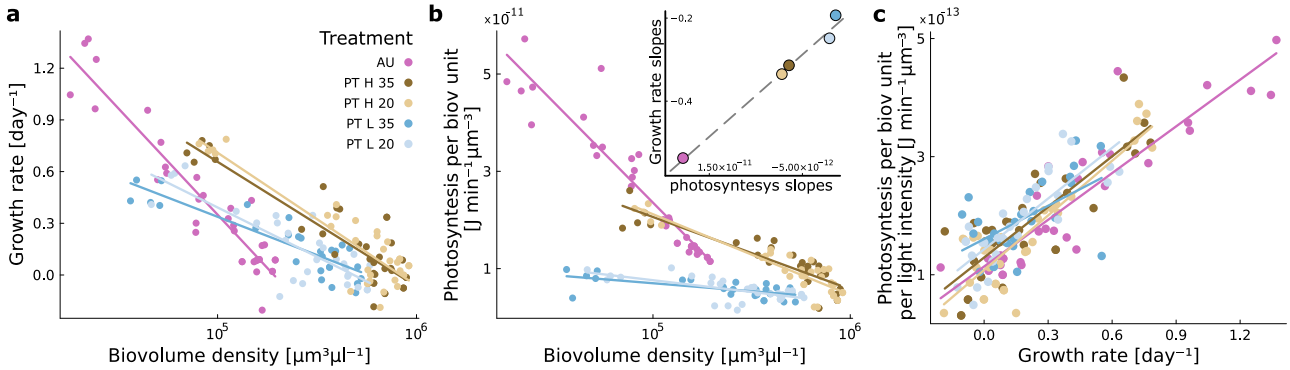

Fig. 4 | Declines in community growth rates mirror reductions in photosynthesis rates across environments. Growth (**a**) and photosynthesis rates per unit biovolume (**b**) decline with total biovolume density at different rates depending on the environment, primarily determined by light availability. All rates are calculated as the geometric mean between consecutive measurements. The insert in (**b**) shows that the rates at which growth and photosynthesis per unit biovolume decline with biomass (slopes) are highly correlated (the broken line has a slope of 1). **c** Differences in light availability explain variation in both photosynthesis and growth, as these rates converge across all environments once we standardise photosynthesis for light intensity. Colours identify the treatment based on geographic location (AU = Australia, PT = Portugal), light (High vs Low) and salinity (35 vs 20 ppt). Source data are provided as a Source Data file.

on body size properties (i.e., classic organismal metabolism-size relationships). However, the (mostly) sublinear scaling between individual metabolism or production with body size collapses onto isometric (linear) scaling when we compare species at equivalent biomass densities. Thus, competition with an equal amount of biomass alters individual scalings in a defined and predictable way that holds across species, growth phases and environments, and is independent of the composition of the biomass. This result solves some of the inconsistencies and variability in metabolic scalings[21,29,35–38] (reviewed in refs. 10,26) and shows how essential it is to account for changes in metabolism in response to competition when estimating scaling exponents.

Many species show metabolic density-dependence in response to intraspecific competition, including prokaryotes[39], unicellular[18,21] and multicellular eukaryotes[17,22]. The effects of interspecific competition on metabolism, however, have been explored in a handful of studies[13,40], so it is difficult to predict how competition between species affects community functioning. If species in a community compete for similar resources, it might not be surprising that their metabolism and growth decline with increasing (biomass) competition from other species. What is surprising is that community composition only minimally influences these metabolic declines. While our communities are less diverse than natural systems, we intentionally chose phytoplankton species from different functional groups, with different sizes (3 orders of magnitude) and pigments that are known to mediate competitive interactions[41–43]. The general effects of biomass competition seem to prevail over these species-specific traits.

One exception is for photosynthesis. Community photosynthesis was estimated more precisely from species-specific rates (rather than a species-naïve "general" approach), possibly because some of our species can obtain energy from different sources (e.g., *Amphidinium* may also function as a mixotroph[44]) or have different capacity to intake or store resources (which can be size-dependent)[30,42]. Photosynthesis rates, indeed, tend to have an unimodal distribution with cell size, which indicates that species of intermediate sizes have higher photosynthetic rates than smaller or larger phytoplankton[30]. Therefore, per capita photosynthetic rates might respond differently to increases in conspecific or heterospecific biomass, affecting community predictions. These species-specific differences were less apparent for respiration and growth.

A limitation of working with phytoplankton is that we cannot measure the metabolism of single cells in isolation ($N = 1$); we need to estimate it from a population measurement. Despite the variability in scaling exponents reported for phytoplankton, a recent review indicates that photosynthesis and respiration scale mostly sublinearly with cell size across algal phyla[26]. The per-cell scaling exponents we obtain when rescaling at the same population densities are clearly sublinear for photosynthesis and growth but are more variable for respiration. This variability might be explained by a combination of stressful environmental conditions (metabolic scaling relationships often differ between environments[28,45]) and greater experimental error on respiration rates which are lower than photosynthesis rates in an absolute sense. To explore the generality of our results, we manipulated two environmental factors (light and salinity) that are important for phytoplankton, but we cannot extrapolate how biomass competition affects metabolism-size scaling in other environments. Nonetheless, our data track the entire growth process of communities, from far to equilibrium until carrying capacity spanning different growth phases and nutrient regimes. The effects of biomass competition on individual metabolism-size relationships were consistent across all of them (Fig. 2).

Importantly our results do not mean that all species in a community are equally affected by the biomass of intra- and inter-specific competitors. To test this, we would need to measure the metabolic response of individual species in a community which is experimentally unavailable. Competition theory and research suggest that intraspecific competition is often stronger than interspecific competition[34,46], so we would expect differences in how species metabolism responds to intra- and inter-specific competitors. Our results suggest that even if there are differences in species responses, these balance each other out at the community level or are sufficiently small that they can be ignored. This result, while it also shows that populations growth sublinearly, is not compatible with the sublinear growth model presented in Hatton et al.[7]; in their model, density-dependence is given by the biomass of conspecifics only, while interspecific competitors affect growth with a different functional form which is not what we observe.

Phytoplankton species compete for similar and essential resources (light and nutrients), so this system might show a strong level of community regulation that might be weaker for species that use substitutable resources. Nonetheless, our simplified system shows similar patterns (no effect of species size on community rates) to those observed in a variety of ecosystems at or near carrying capacity[3,47], including phytoplankton communities in nature[29], mesocosms[48], or over longer successional trajectories in the laboratory[13]. This consistency suggests that species interactions, such as competition for resources, can lead to strong regulation of community functioning so that community-level patterns are more consistent than those at the

individual or population level[8]. We look forward to studies that test these ideas in organisms that compete for non-essential resources and for which metabolism can be measured individually.

In conclusion, we find that increases in total biomass lead to consistent changes in metabolism across species that are interacting in a community. We do not know the specific mechanism behind these responses, but ecosystems can display allometric patterns of resource transport efficiency similar to size-dependent patterns of organismal metabolism[1,4]. So the generalised metabolic decline we observe with biomass might emerge because of geometric factors (increases in total biomass density alter the flow of resources according to common organising principles)[1,4] and behavioural or physiological adjustments to biomass density that are similar between species[17,19,21–23,49,50]. The resulting scaling patterns might thus be independent of the specific nature of interactions, at least when species compete for similar resources[8,51]. We offer the first empirical demonstration of this hypothesis[8] and show that community functioning is tightly integrated – to the point that extending the relationship between metabolism and mass from organisms to entire communities can give a reliable representation of community functioning.

Methods

Experimental setups

We combined two geographically distinct datasets of marine phytoplankton. Both datasets used species of marine phytoplankton obtained from culture collections; species were cultured in temperature-controlled rooms at 22 ± 1 °C using autoclaved Guillard's f/2 medium, prepared with filtered natural seawater.

The first dataset (AU) is from Ghedini et al.[20], where they grew five species of marine phytoplankton in three species diversity treatments over 10 days: monoculture, pairs or communities with all five species. Each monoculture and species pair were replicated three times and communities five times ($N = 50$ cultures). The work was performed at Monash University, Australia, and the species were obtained from the Australian National Algae Culture Collection: *Amphidinium carterae* (CS-740), *Tetraselmis* sp. (CS-91), *Dunaliella tertiolecta* (CS-14), *Tisochrysis lutea* (CS-177) and *Synechococcus* sp. (CS-94). All cultures were placed in cell culture flasks filled to 100 ml and grown on a 14–10 hr light-dark cycle under non-saturating irradiance levels (115 µmol photons m^{-2} s^{-1}) at ambient salinity (35 ppt). Flasks were shaken and randomly rearranged on the shelves every day. Nutrients were added daily by replacing 10% of the medium from each flask with fresh f/2 medium. All cultures were started with an initial total biovolume ~ 6×10^8 µm^3 (~ 10^3 µm^3 µl^{-1}), where biovolume is the product of cell size (volume) and number of cells and is used as a proxy for biomass in phytoplankton. Cultures were sampled on each day for the first five days and on alternate days afterwards for a total of eight sampling times (days 0, 1, 2, 3, 4, 6, 8, 10).

The second dataset (PT, unpublished) was collected at the Instituto Gulbenkian de Ciência (previously IGC, now GIMM) in Portugal using five phytoplankton species obtained from the Roscoff Culture Collection (France): *Amphidinium carterae* (RCC88), *Dunaliella tertiolecta* (RCC6), *Phaeodactylum tricornutum* (RCC2967), *Tisochrysis lutea* (RCC90), *Nannochloropsis granulata* (RCC438). These species were grown either alone in monoculture or together in a community for 16 days under two levels of salinity (35 or 20 ppt) and light (60 or 30 µmol photons m^{-2} s^{-1}) in cross combination to simulate a gradient of stressful environments. We set up 5 replicate communities (a mix of the five species in equal biovolumes) and 2 replicate monocultures of each species for each level of salinity and light in glass bottles filled with 200 ml ($N = 60$ cultures). The position of the cultures was randomised at each sampling day and cultures were bubbled continuously for mixing. We started with an initial total biovolume of ~ 4×10^9 µm^3 (~ 10^3 µm^3 µl^{-1}) for each treatment. We tracked changes in the abundance, size, and biovolume of species over time through microscopy; concomitantly, we measured the metabolism of monocultures and communities using respirometry (photosynthesis and respiration). We maintained salinity treatments by adding small amounts of distilled water when needed. Communities and monocultures were sampled on 7 and 6 occasions, respectively, over the course of 16 days to measure changes in biovolume and metabolism as detailed below (days 2-5-7-9-13-15 for monocultures, 2-3-7-9–12-14-16 for communities).

Cell size, population and biovolume density

In both experiments, 1 ml of sample from each culture was fixed with 1% Lugol's solution to quantify cell size and abundance. From these fixed samples, we loaded 10 µl onto a cell counting chamber (Neubauer improved), and we took photos of the sample with an Olympus IX73 inverted microscope using 400x magnification. Photos were processed in Fiji/ImageJ[52] to quantify the cell volume (µm^3), number of cells of each species (µl^{-1}), and biovolume as their product (µm^3 µl^{-1}). Cell volume was calculated from the major and minor axis of each cell by assigning to each species an approximate geometric shape (prolate spheroid for all species, except *Synechococcus*, *Tisochrysis*, and *Nannochloropsis* for which we assumed a spherical shape)[53]. The total biovolume of species mixtures (pairs or communities) was calculated as the sum of each individual species' biovolume.

Metabolism

Photosynthesis and respiration rates were measured from changes in percentage oxygen saturation under light (photosynthesis) or dark conditions (respiration) using 24-channel sensor dish readers (SDR; PreSens Precision Sensing GmbH, Germany). Measurements were performed in 5 ml (AU) or 2 ml (PT) glass vials with integrated oxygen sensors approximately in the middle of the photoperiod.

The system was calibrated with 100% and 0% oxygenated water prior to each experiment. We quantified photosynthesis as the rate of oxygen production under the same light intensity at which the cultures were grown, over a period of 30 min or less if cultures approached 250% earlier (the maximum value the instrument can read). Respiration was quantified as the rate of oxygen decline over 30 min following light exposure. We added a 2% solution of sodium bicarbonate to each vial to avoid carbon limitation during photosynthesis. We added blanks prepared with the supernatant of the samples on each SDR reader to account for drift and bacterial respiration (12 and 24 each sampling day for the two datasets, respectively).

In both experiments, the rate of photosynthesis or respiration of the whole sample (VO_2; units µmol O_2/min) was measured as $VO_2 = 1 \times ((m_a m_b)/100 \times V\beta O_2)$ following[54], where m_a is the rate of change of O_2 saturation in each sample (min^{-1}), m_b is the mean O_2 saturation across all blanks (min^{-1}), V is the sample volume in litres and βO_2 is the oxygen capacity of air-saturated seawater for the temperature and salinity of the sample (µmol O_2/L). The first three minutes of measurements were discarded for all samples for photosynthesis. Respiration rates were calculated after 10 min of dark when rates showed a linear decline. Rates of photosynthesis and respiration (µmol O_2/min) were converted to calorific energy (J/min) using the conversion factor of 0.512 J/µmol O_2[55] to estimate energy production and energy consumption, respectively, as in previous work[56].

Data analysis

Data were analysed and visualised through a Julia pipeline, using linear mixed effect models in RStudio (version 4.3.1) to test for differences in exponents and intercepts.

1. Data filtering: We discard negative respiration measures. Negative values of respiration are obtained when the slope of the blanks is steeper than that of the sample, which indicates either some error in the preparation/seal of the vial or that the sample does not contain enough (live) phytoplankton biomass to differentiate their respiration from that of bacteria (blanks). The number of

discarded samples is: 12/197 (PT monocultures), 11/279 (PT communities), and none in the other dataset: 0/105 (AU monocultures), 0/210 (AU pairs), 0/35 (AU communities). Similarly, we discard negative photosynthesis values (38 in total: 24 PT monocultures, 14 PT communities). We also removed day 0 for all analyses as we did not have metabolic data on that first day.

2. Data normalisation: Respiration rates, photosynthesis rates, and total biovolume values are normalised by the sample volume (2 ml for PT data, 5 ml for AU data), so they are reported in J min^{-1} μl^{-1} or μm^3 μl^{-1} respectively.
3. Growth rate: Calculated as $g_{l,t} = \frac{\ln(B_{l,t'}/B_{l,t})}{t'-t}$. Where $B_{l,t}$ and $B_{l,t'}$ are two total biovolume measurements performed on sample l at time t and $t' > t$. For the AU experiment, we calculated growth based on 90% of the previous biovolume because, on each sampling day, we removed 10% of the sample.
4. Scaling of community/population rates to total biovolume and the effect of species size on these rates: We fit a linear relationship between the logarithm of respiration (photosynthesis) rates and the logarithm of biovolume density. Still, we do not assume that there is an intrinsic power law relationship between these two quantities. In fact, the growth in biovolume we observe for each replicate is smaller than two orders of magnitude, not allowing us to establish a reliable functional form. Nonetheless, the log-log relationship allows us to find a functional form enabling the following analysis. For all analyses below, we used linear mixed-effect models, including sample ID (code) as a random effect to account for repeated measures. Respiration, photosynthesis, and biovolume were $\log_{10}$-transformed prior to analyses. Growth was analysed untransformed using the geometric mean of biovolume (ln-transformed); this fits a Gompertz growth function which seems to fit our data better than a power law or GLV. The fits were done by grouping data in the following ways:
   a – Overall scaling of monocultures and communities (Fig. 1 and Supplementary Fig. 1a): we use total respiration (photosynthesis, growth) as response variable and the interaction between total biovolume and scale (monocultures, communities) as predictors. Species pairs are excluded from this analysis because they are present in only one environment (AU, see analysis below). We also test for the effect of species size on each rate, including average size ($\log_{10}$-transformed) as the predictor, on the combined monoculture and community data.
   b – Differences in scaling between environments (Supplementary Figs. 1, 2): we analysed the data separately for each geographic location. We used linear mixed-effect models, including the interaction between biovolume and scale (monocultures, pairs, communities) for AU data. For PT data, we used biovolume, scale (monocultures, communities) and treatment (orthogonal combinations of low/high light and 20/35ppt salinity) as predictors. Interactions were removed when $p > 0.25$.
5. Species-specific scalings: We used monoculture data to estimate the relationship between respiration (photosynthesis, growth) and total biovolume for each strain in each environment (Supplementary Fig. 3 and Supplementary Table 4). While some species are the same in the two datasets (i.e., *Amphidinium*, *Dunaliella*, *Tisochrysis*), they are different strains (genetically and geographically distinct). Thus, we consider them independently. We use the ordinary least squares method (OLS) which is recommended when the error on the x-axis (biovolume) is smaller than the error on the y-axis (metabolism) and consistent with previous work[3]. We test the effect of size on monoculture rates using average size ($\log_{10}$-transformed) and geographic location (AU, PT) as predictors (Supplementary Fig. 5 and Supplementary Table 5).
6. Rescaled individual metabolic rate at fixed biovolume or cell density: Here, we want to evaluate the slope of metabolism-size relationships when species are at the same biovolume or cell density. To do this, we use the monoculture data to rescale the respiration (photosynthesis, growth) rate of each species (at the population level) to the value predicted at a fixed biovolume. To do this, we use a species and environment-specific scaling (obtained in 5; reported in Supplementary Table 4). In this way, every datapoint k of species s was rescaled independently as $E_k^* = E_k \cdot \left(\frac{B^*}{B_k}\right)^{\alpha_{h,s}}$ where E_k is the measured respiration rate of datapoint k, B_k is the measured total biovolume, B^* is the target (fixed) biovolume density (10^5 μm^3 μl^{-1}), and $\alpha_{h,s}$ is the exponent of the power law fitted at fixed environment h and species s. Such rescaling keeps the spread of the data on the y-axis (respiration rates) intact while removing variation on the x-axis (biovolume). The same procedure can be performed to fix the cell density N^* to a value $\widetilde{E}_k^* = E_k \cdot \left(\frac{N^*}{N_k}\right)^{\alpha_{h,s}}$. We can rescale by density using the exponent of the biovolume dependence as $\frac{N^*}{N_k} = \frac{N^* \bar{S}_s}{N_k \bar{S}_s} = \frac{B_s^*}{B_{k,s}}$. We used a biovolume density of 10^5 μm^3 μl^{-1}, which was in the centre of the range for Fig. 2. Similarly, we rescaled metabolic rates to a population density of 10^4 cells μl^{-1} which was a compromise between small and large species. We used a population density of 10^3 for growth as the larger species had many negative values at 10^4. We report the values of the scaling exponents obtained for a wider range of biovolumes and population densities (relevant to our cultures) in Supplementary Fig. 10.
   Average individual respiration rate: by rescaling the total biovolume to a fixed value, we lost the information on the total number of individuals. We know both B^* and the average size of each species for each datapoint $\bar{S}_k$, thus the number of individuals is $N_k(B^*) = \frac{B^*}{\bar{S}_k}$. We thus divide the total respiration rates at fixed biovolume E_k^* by $N_k(B^*)$ to calculate individual respiration rates at each timepoint. Finally, we estimate the scaling exponent of the relationship between rescaled cell rates and cell size (Fig. 2) using linear mixed-effect models (with code as a random effect). Data were analysed separately for AU and PT data as the latter also included a size by treatment interaction (light and salinity). All rates were $\log_{10}$-transformed, including individual biovolume production.
7. Predictions of community rates from monoculture rates:
   a – Respiration and photosynthesis rates per unit of biovolume: We divide the measured respiration rates of each datapoint by the total biovolume $e_k := \frac{E_k}{B_k}$. We then fit a linear relationship between the logarithm of rates per unit of biovolume and the logarithm of biovolume density. Here we fit the data by grouping for (i) species and environment (species-specific scaling; note that these scalings are simply the ones obtained in point 5 minus one that is $\alpha_{h,s} - 1$), or (ii) environment only (general scaling).
   b – Predict community rates from monoculture data: We use the relationship between Respiration/photosynthesis rate per unit of biovolume and population biovolume density obtained for monocultures (point 7a) to predict the metabolism per unit of biovolume in each community with three methods:
   - Conspecifics: we use the fits defined in 7a-i (environment and species) to calculate the metabolic rate of biovolume for each species and in each environment from the biovolume density of conspecifics present in the community at each time point. This approach assumes that the metabolism of a species is only responsive to the presence of conspecifics, while other species have no effect. We then sum over all species to find the community total metabolism.
   - Whole community: we use the same fits above (environment and species, 7a-i) to calculate the metabolic rate of

biovolume for each species and in each environment from the total biovolume density of the community at each time point. This approach assumes that the metabolism of a species is equally affected by competitors, independently of their nature – it does not matter who your competitors are, only how much biomass density surrounds you. We then sum over all species to find community total metabolism;

- General scaling: we use a general (not species-specific) relationship between metabolism per unit of biovolume and biovolume that varies between environments; we calculate it grouping by environment only (7a-ii). This approach assumes that the metabolism of a species is affected by biovolume in a way that is species-independent. Identity does not matter; competition affects everyone in the same way.

To estimate community growth we use directly the fits obtained in point 5 (species by environment) because growth is already per unit of biovolume. The "general" scaling was calculated for growth in a similar way as above, i.e., grouping by environment only.

c – Predictions of community metabolism (respiration or photosynthesis) based on species pairs*:* We calculate the effect of intraspecific competition in species pairs by fitting the difference between the expected metabolism per unit of biovolume of each species s in each datapoint k (based on monoculture data) $e_{s,k,predicted} \sim B_{s,k}^{\alpha_{h,s}-1}$ and the average metabolism per unit of biovolume measured on pairs $e_{tot,k,measured} = \frac{E_{tot,k,measured}}{B_{tot,k,measured}}$, where $B_{tot,k} = B_{s,k,measured} + B_{p,k,measured}$ and $E_{tot,k} = E_{s,k} + E_{p,k}$ but for metabolism E we cannot know the relative contribution of species s and species p (we can only measure the total).

Specifically, we fit a linear relationship to the distribution of points with coordinates:

$$X = \log(B_{tot,k,measured}) - \log(B_{s,k,measured})$$

$$Y = \log(e_{tot,k,measured}) - \log(e_{s,k,predicted})$$

In this way, we can estimate the effect of each species on each other, obtaining the slopes $\gamma_{p,s}$ that express the effect of the species p on species s. The obtained values are used to estimate the effect of *all* interspecific competitors on the metabolism per unit biovolume of each species in a community as

$$e_{s,k,all} = e_{s,k,predicted} \cdot \prod_{p \neq s} \left(\frac{B_s + \sum_{j=1}^{p} B_j}{B_s + \sum_{j=1}^{p-1} B_j} \right)^{\gamma_{p,s}} \quad (4)$$

The total community rates are then obtained by summing the contribution of each species as $E_{k,predicted} = \sum_{s=1}^{n} e_{s,k,all} B_{s,k,measured}$.

d – Predictions of community growth rates based on species pairs*:* we calculate the effect of intraspecific competition in species pairs by fitting the difference between the expected growth of each species s in each data point k (based on monoculture data) $g_{s,k,predicted} \sim B_{s,k} \alpha_{h,s}$ and the average growth measured on pairs $g_{tot,k,measured}$ calculated as in point 3 above. Then, we fit a linear relationship to the distribution of points with coordinates:

$$X = \log(B_{tot,k,measured}) - \log(B_{s,k,measured})$$

$$Y = g_{tot,k,measured} - g_{s,k,predicted}.$$

In this way, we can estimate the effect of each species on each other, obtaining the slopes $\gamma_{p,s}$ that express the effect of the species p on species s. The obtained values are used to estimate the effect of *all* interspecific competitors on the metabolism per unit biovolume of each species in a community as

$$g_{s,k,all} = g_{s,k,predicted} + \sum_{p \neq s} \left[\ln\left(B_s + \sum_{j=1}^{p} B_j\right) - \ln\left(B_s + \sum_{j=1}^{p-1} B_j\right) \right] \quad (5)$$

The total community rates are then obtained by summing the contribution of each species as $g_{k,predicted} = \frac{\sum_s g_{s,k,all} B_{s,k,measured}}{\sum_s B_{s,k,measured}}$.

e – Prediction error*:* We calculated the difference (delta) between the estimates obtained above and the empirical measures of community rates (on a log scale for respiration and photosynthesis) to visualise the offset of the prediction for each hypothesis.

f – Randomisation: We randomised the association between biovolumes and species-specific scalings by shuffling the exponents $\alpha_{h,s}$ across species as $\alpha_{h,p(s)}$, where $p(s)$ is the reshuffling function of species s. Than predictions are made as $E_k \sim \sum_s B_{s,k} B_{tot,k}^{\alpha_{h,p(s)}-1}$ for metabolism. We used a similar approach for growth.

8. Relationship between photosynthesis and growth across environments: We calculate the geometric mean of photosynthesis rates per unit biovolume between consecutive measurements to have a quantity relatable to the average growth rate (which is also calculated between consecutive measurements, point 3). We then plot the relationship between photosynthesis per unit biovolume (geom. mean) and biovolume density, and between growth and biovolume density. Here biovolume is also the geometric mean and is $\log_{10}$-transformed in both cases. Finally, to highlight the connection between these rates and account for differences in light intensity between treatments, we normalise photosynthesis by light intensity and plot it against growth.

Reporting summary

Further information on research design is available in the Nature Portfolio Reporting Summary linked to this article.

Data availability

All data used and generated in this study have been deposited in the Figshare database under the accession code https://doi.org/10.6084/m9.figshare.25234837. The dataset previously used for reference 20 (Ghedini et al.[20] Func. Ecol.) is also accessible on Figshare at https://doi.org/10.26180/16665964. Source data are provided in this paper.

Code availability

All code used in this study is available on Figshare: https://doi.org/10.6084/m9.figshare.25234837.

References

1. Nidzieko, N. J. Allometric scaling of estuarine ecosystem metabolism. *Proc. Natl. Acad. Sci. USA* **115**, 6733–6738 (2018).
2. Perkins, D. M. et al. Consistent predator-prey biomass scaling in complex food webs. *Nat. Commun.* **13**, 4990 (2022).
3. Hatton, I. A. et al. The predator-prey power law: Biomass scaling across terrestrial and aquatic biomes. *Science* **349**, https://doi.org/10.1126/science.aac6284 (2015).
4. Garlaschelli, D., Caldarelli, G. & Pietronero, L. Universal scaling relations in food webs. *Nature* **423**, 165–168 (2003).
5. Cebrian, J. Energy flows in ecosystems. *Science* **349**, 1053–1054 (2015).
6. White, C. R., Alton, L. A., Bywater, C. L., Lombardi, E. J. & Marshall, D. J. Metabolic scaling is the product of life-history optimization. *Science* **377**, 834–839 (2022).

7. Hatton, I. A., Mazzarisi, O., Altieri, A. & Smerlak, M. Diversity begets stability: Sublinear growth and competitive coexistence across ecosystems. *Science* **383**, eadg8488 (2024).
8. Loreau, M. In *Unsolved Problems in Ecology* (eds. Tilman, G. D., Dobson, A. & Holt, R. D.) 218–224 (Princeton University Press, 2020).
9. Wickman, J., Litchman, E. & Klausmeier, C. A. Eco-evolutionary emergence of macroecological scaling in plankton communities. *Science* **383**, 777–782 (2024).
10. Hatton, I. A., Dobson, A. P., Storch, D., Galbraith, E. D. & Loreau, M. Linking scaling laws across eukaryotes. *Proc. Natl. Acad. Sci. USA* **116**, 21616 (2019).
11. Kleiber, M. Body size and metabolism. *Hilgardia* **6**, 315–351 (1932).
12. Brown, J. H., Gillooly, J. F., Allen, A. P., Savage, V. M. & West, G. B. Toward a metabolic theory of ecology. *Ecology* **85**, 1771–1789 (2004).
13. Ghedini, G., Malerba, M. E. & Marshall, D. J. How to estimate community energy flux? A comparison of approaches reveals that size-abundance trade-offs alter the scaling of community energy flux. *Proc. R. Soc. Biol. Sci.* **287**, 20200995 (2020).
14. Antunes, A. C. et al. Environmental drivers of local abundance–mass scaling in soil animal communities. *Oikos* **2023**, e09735 (2023).
15. de Castro, F. & Gaedke, U. The metabolism of lake plankton does not support the metabolic theory of ecology. *Oikos* **117**, 1218–1226 (2008).
16. Cyr, H. & Pace, M. L. Allometric theory: Extrapolations from individuals to communities. *Ecology* **74**, 1234–1245 (1993).
17. DeLong, J. P., Hanley, T. C. & Vasseur, D. A. Competition and the density dependence of metabolic rates. *J. Anim. Ecol.* **83**, 51–58 (2014).
18. DeLong, J. P. & Hanson, D. T. Metabolic rate links density to demography in Tetrahymena pyriformis. *ISME J.* **3**, 1396–1401 (2009).
19. Ghedini, G., White, C. R. & Marshall, D. J. Does energy flux predict density-dependence? An empirical field test. *Ecology* **98**, 3116–3126 (2017).
20. Ghedini, G., Marshall, D. J. & Loreau, M. Phytoplankton diversity affects biomass and energy production differently during community development. *Funct. Ecol.* **36**, 446–457 (2022).
21. Malerba, M. E., White, C. R. & Marshall, D. J. Phytoplankton size-scaling of net-energy flux across light and biomass gradients. *Ecology* **98**, 3106–3115 (2017).
22. Nadler, L. E., Killen, S. S., McClure, E. C., Munday, P. L. & McCormick, M. I. Shoaling reduces metabolic rate in a gregarious coral reef fish species. *J. Exp. Biol.* **219**, 2802–2805 (2016).
23. Nørgaard, L. S., Ghedini, G., Phillips, B. L. & Hall, M. D. Energetic scaling across different host densities and its consequences for pathogen proliferation. *Funct. Ecol.* **35**, 475–484 (2021).
24. Malerba, M. E. & Marshall, D. J. Size-abundance rules? Evolution changes scaling relationships between size, metabolism and demography. *Ecol. Lett.* **22**, 1407–1416 (2019).
25. Field, C. B., Behrenfeld, M. J., Randerson, J. T. & Falkowski, P. Primary production of the biosphere: Integrating terrestrial and oceanic components. *Science* **281**, 237 (1998).
26. Hillebrand, H. et al. Cell size as driver and sentinel of phytoplankton community structure and functioning. *Funct. Ecol.* **36**, 276–293 (2022).
27. Finkel, Z. V. et al. Phytoplankton in a changing world: cell size and elemental stoichiometry. *J. Plankton Res.* **32**, 119–137 (2010).
28. Gjoni, V., Glazier, D. S., Wesner, J. S., Ibelings, B. W. & Thomas, M. K. Temperature, resources and predation interact to shape phytoplankton size–abundance relationships at a continental scale. *Glob. Ecol. Biogeogr.* **32**, 2006–2016 (2023).
29. Huete-Ortega, M., Cermeño, P., Calvo-Díaz, A. & Marañón, E. Isometric size-scaling of metabolic rate and the size abundance distribution of phytoplankton. *Proc. R. Soc. B Biol. Sci.* **279**, 1815–1823 (2011).
30. Marañón, E. Cell size as a key determinant of phytoplankton metabolism and community structure. *Annu. Rev. Mar. Sci.* **7**, 241–264 (2015).
31. Tatsumi, S. & Loreau, M. Partitioning the biodiversity effects on productivity into density and size components. *Ecol. Lett.* **26**, 1963–1973 (2023).
32. Glazier, D. S. Beyond the '3/4-power law': variation in the intra-and interspecific scaling of metabolic rate in animals. *Biol. Rev.* **80**, 611–662 (2005).
33. López-Sandoval, D. C., Rodríguez-Ramos, T., Cermeño, P., Sobrino, C. & Marañón, E. Photosynthesis and respiration in marine phytoplankton: Relationship with cell size, taxonomic affiliation, and growth phase. *J. Exp. Mar. Biol. Ecol.* **457**, 151–159 (2014).
34. Adler, P. B. et al. Competition and coexistence in plant communities: intraspecific competition is stronger than interspecific competition. *Ecol. Lett.* **21**, 1319–1329 (2018).
35. Long, Z. T. & Morin, P. J. Effects of organism size and community composition on ecosystem functioning. *Ecol. Lett.* **8**, 1271–1282 (2005).
36. Makarieva, A. M. et al. Mean mass-specific metabolic rates are strikingly similar across life's major domains: Evidence for life's metabolic optimum. *Proc. Natl. Acad. Sci. USA* **105**, 16994–16999 (2008).
37. Finkel, Z. V., Irwin, A. J. & Schofield, O. Resource limitation alters the ¾ size scaling of metabolic rates in phytoplankton. *Mar. Ecol. Prog. Ser.* **273**, 269–280 (2004).
38. Marañón, E., Cermeño, P., Rodríguez, J., Zubkov, M. V. & Harris, R. P. Scaling of phytoplankton photosynthesis and cell size in the ocean. *Limnol. Oceanogr.* **52**, 2190–2198 (2007).
39. An, J. H., Goo, E., Kim, H., Seo, Y.-S. & Hwang, I. Bacterial quorum sensing and metabolic slowing in a cooperative population. *Proc. Natl. Acad. Sci. USA* **111**, 14912–14917 (2014).
40. Janča, M. & Gvoždík, L. Costly neighbours: Heterospecific competitive interactions increase metabolic rates in dominant species. *Sci. Rep.* **7**, 5177 (2017).
41. Gallego, I., Venail, P. & Ibelings, B. W. Size differences predict niche and relative fitness differences between phytoplankton species but not their coexistence. *ISME J.* **13**, 1133–1143 (2019).
42. Litchman, E., Klausmeier, C. A., Schofield, O. M. & Falkowski, P. G. The role of functional traits and trade-offs in structuring phytoplankton communities: scaling from cellular to ecosystem level. *Ecol. Lett.* **10**, 1170–1181 (2007).
43. Papanikolopoulou, L. A. et al. Interplay between r- and K-strategists leads to phytoplankton underyielding under pulsed resource supply. *Oecologia* **186**, 755–764 (2018).
44. Karafas, S., Teng, S. T., Leaw, C. P. & Alves-de-Souza, C. An evaluation of the genus *Amphidinium* (Dinophyceae) combining evidence from morphology, phylogenetics, and toxin production, with the introduction of six novel species. *Harmful Algae* **68**, 128–151 (2017).
45. Glazier, D. S. Variable metabolic scaling breaks the law: from 'Newtonian' to 'Darwinian' approaches. *Proc. R. Soc. B Biol. Sci.* **289**, 20221605 (2022).
46. Chesson, P. Mechanisms of maintenance of species diversity. *Annu. Rev. Ecol. Syst.* **31**, 343–366 (2000).
47. Waters, J. S., Holbrook, C. T., Fewell, J. H. & Harrison, J. F. Allometric scaling of metabolism, growth, and activity in whole colonies of the seed-harvester ant pogonomyrmex californicus. *Am. Nat.* **176**, 501–510 (2010).
48. Padfield, D., Buckling, A., Warfield, R., Lowe, C. & Yvon-Durocher, G. Linking phytoplankton community metabolism to the individual size distribution. *Ecol. Lett.* **21**, 1152–1161 (2018).

49. Poulson-Ellestad, K. L. et al. Metabolomics and proteomics reveal impacts of chemically mediated competition on marine plankton. *Proc. Natl. Acad. Sci. USA* **111**, 9009 (2014).
50. Sjöberg, M., Albrectsen, B. & Hjältén, J. Truncated power laws: a tool for understanding aggregation patterns in animals? *Ecol. Lett.* **3**, 90–94 (2000).
51. Narla, A. V., Hwa, T. & Murugan, A. Dynamic coexistence driven by physiological transitions in microbial communities. Preprint at http://biorxiv.org/lookup/doi/10.1101/2024.01.10.575059 (2024).
52. Schindelin, J. et al. Fiji: an open-source platform for biological-image analysis. *Nat. Methods* **9**, 676–682 (2012).
53. Hillebrand, H., Dürselen, C.-D., Kirschtel, D., Pollingher, U. & Zohary, T. Biovolume calculation for pelagic and benthic microalgae. *J. Phycol.* **35**, 403–424 (1999).
54. White, C. R., Kearney, M. R., Matthews, P. G. D., Kooijman, S. A. L. M. & Marshall, D. J. A manipulative test of competing theories for metabolic scaling. *Am. Nat.* **178**, 746–754 (2011).
55. Williams, P. J., le, B. & Laurens, L. M. L. Microalgae as biodiesel & biomass feedstocks: Review & analysis of the bio-chemistry, energetics & economics. *Energy Environ. Sci.* **3**, 554–590 (2010).
56. Ghedini, G., Loreau, M. & Marshall, D. J. Community efficiency during succession: a test of MacArthur's minimisation principle in phytoplankton communities. *Ecology* **101**, e03015 (2020).

Acknowledgements

We are grateful to Michel Loreau, Jacopo Grilli, Onofrio Mazzarisi, and Isabel Gordo for their comments on an earlier version of this manuscript. We thank Moritz Klassen for help with data collection and the Imaging Facility of the Gulbenkian Institute for Molecular Medicine (GIMM, particularly José Marques) for assistance with image processing. This work was supported by a postdoctoral PONTE fellowship from the Fundação Calouste Gulbenkian-IGC to L.F. and a fellowship from "la Caixa" Foundation (LCF/BQ/PI21/11830001; ID 100010434) and the European Union's Horizon 2020 research and innovation programme under the Marie Sklodowska Curie grant agreement no. 847648 to G.G. G.G. is also supported by an ERC Starting Grant funded by the European Union (ERC, META_FUN, 101116029). Views and opinions expressed are however those of the author(s) only and do not necessarily reflect those of the European Union or the European Research Council. Neither the European Union nor the granting authority can be held responsible for them.

Author contributions

L.F. and G.G. conceived the idea for this manuscript. G.G. designed and performed the experiments. L.F. and G.G. analysed the data. G.G. drafted the manuscript and both authors contributed to the final version.

Competing interests

The authors declare no competing interests.

Additional information

Supplementary information The online version contains supplementary material available at https://doi.org/10.1038/s41467-024-54307-w.

Correspondence and requests for materials should be addressed to Lorenzo Fant or Giulia Ghedini.

Peer review information *Nature Communications* thanks Daniel Perkins and the other anonymous reviewers for their contribution to the peer review of this work. A peer review file is available.

Reprints and permissions information is available at http://www.nature.com/reprints

Publisher's note Springer Nature remains neutral with regard to jurisdictional claims in published maps and institutional affiliations.

Open Access This article is licensed under a Creative Commons Attribution-NonCommercial-NoDerivatives 4.0 International License, which permits any non-commercial use, sharing, distribution and reproduction in any medium or format, as long as you give appropriate credit to the original author(s) and the source, provide a link to the Creative Commons licence, and indicate if you modified the licensed material. You do not have permission under this licence to share adapted material derived from this article or parts of it. The images or other third party material in this article are included in the article's Creative Commons licence, unless indicated otherwise in a credit line to the material. If material is not included in the article's Creative Commons licence and your intended use is not permitted by statutory regulation or exceeds the permitted use, you will need to obtain permission directly from the copyright holder. To view a copy of this licence, visit http://creativecommons.org/licenses/by-nc-nd/4.0/.

© The Author(s) 2024